ELSEVIER

Contents lists available at ScienceDirect

Applied Mathematics and Computation

journal homepage: www.elsevier.com/locate/amc



Numerical studies of the Steklov eigenvalue problem via conformal mappings



Weaam Alhejaili^{a,b}, Chiu-Yen Kao^{c,1,*}

- ^a Institute of Mathematical Sciences, Claremont Graduate University, Claremont, CA 91711, USA
- b Department of Mathematical Sciences, College of Sciences, Princess Nourah bint Abdulrahman University, Riyadh, Saudi Arabia
- ^c Department of Mathematical Sciences, Claremont McKenna College, Claremont, CA 91711, USA

ARTICLE INFO

Keywords: Steklov eigenvalues Extremal eigenvalue problem Shape optimization Spectral method Conformal mapping

ABSTRACT

In this paper, spectral methods based on conformal mappings are proposed to solve the Steklov eigenvalue problem and its related shape optimization problems in two dimensions. To apply spectral methods, we first reformulate the Steklov eigenvalue problem in the complex domain via conformal mappings. The eigenfunctions are expanded in Fourier series so the discretization leads to an eigenvalue problem for coefficients of Fourier series. For shape optimization problem, we use a gradient ascent approach to find the optimal domain which maximizes kth Steklov eigenvalue with a fixed area for a given k. The coefficients of Fourier series of mapping functions from a unit circle to optimal domains are obtained for several different k.

© 2018 Elsevier Inc. All rights reserved.

1. Introduction

The second order Steklov eigenvalue problem satisfies

$$\begin{cases} \Delta u(\mathbf{x}) = 0 & \text{in } \Omega, \\ \frac{\partial u}{\partial x} = \lambda u & \text{on } \partial \Omega, \end{cases}$$
 (1)

where \triangle is the Laplace operator acting on the function $u(\mathbf{x})$ defined on $\Omega \subset \mathbb{R}^N$, λ is the corresponding eigenvalue, and $\frac{\partial u}{\partial n} = n \cdot \nabla u$ is the directional derivative in the outward normal direction. Here, we assume that Ω is a bounded open set with Lipschitz boundary $\partial \Omega$. This problem is a simplified version of the mixed Steklov problem which was used to obtain the sloshing modes and frequencies. See Appendix for the derivation of the mixed Steklov problem. The spectral geometry of the Steklov problem has been studied for a long time. See a recent review article on American Mathematical Society (AMS) notice [22] and the references therein. In 2012, Krechetnikov and Mayer were awarded the Ig Nobel prize for fluid dynamics for their work on the dynamic of liquid sloshing. In [25], they studied the conditions under which coffee spills for various walking speeds based on sloshing modes [19].

The Steklov problem (1) has a countable infinite set of eigenvalues which are greater than or equal to zero. We arrange them as $0 = \lambda_0(\Omega) \le \lambda_1(\Omega) \le \lambda_2(\Omega) \le \cdots \le \lambda_k(\Omega) \le \cdots \to \infty$ and denote u_k as the corresponding eigenfunction in

^{*} Corresponding author.

E-mail addresses: weaam.alhejaili@cgu.edu, waalhejali@pnu.edu.sa (W. Alhejaili), ckao@cmc.edu (C.-Y. Kao).

¹ This author's work is supported in part by a collaboration grant for mathematicians from Simons Foundation in 2017–2018 academic year and a NSF grant DMS-1818948.

the Sobolev space $H^1(\Omega)$. The Weyl's law for Steklov eigenvalues [18] states that $\lambda_k \sim 2\pi \left(\frac{k}{|\mathbb{B}^{N-1}||\partial\Omega|}\right)^{\frac{1}{N-1}}$ where \mathbb{B}^{N-1} is the unit ball in \mathbb{R}^{N-1} and $|\cdot|$ denotes the volume of the argument. The variational characterization of the eigenvalues is given by

$$\lambda_k(\Omega) = \min_{v \in H^1(\Omega)} \left\{ \frac{\int_{\Omega} |\nabla v|^2 dx}{\int_{\partial \Omega} v^2 ds} : \int_{\partial \Omega} v u_i ds = 0, \ i = 0, \dots, k - 1 \right\}.$$
 (2)

The eigenfunctions u_k are normalized so that

$$\int_{\partial\Omega} u_k^2 ds = 1. \tag{3}$$

In 1954, Weinstock proved that the disk maximizes the first non-trivial Steklov eigenvalue λ_1 among simply-connected planar domains with a fixed perimeter [17,29]. Furthermore, the kth eigenvalue λ_k for a simply-connected domain with a fixed perimeter is maximized in the limit by a sequence of simply-connected domains degenerating to the disjoint union of k identical disks for any integer $k \ge 1$ [16]. It remains an open question for non-simply-connected bounded planar domains [18]. For maximizing kth Steklov eigenvalue among planar domains with a fixed area, the existence of the optimal shapes was proved in [8, Theorem 6.4] for an optimal open set with a topological boundary of finite Hausdorff measure recently.

Several different numerical approaches were proposed to solve the Steklov eigenvalue problem [1,7] and Wentzell eigenvalue problem [7] which has slightly different boundary conditions. The methods of fundamental solutions were used in [7] to compute the Steklov spectrum and a theoretical error bound were derived. In [1], the authors used a boundary integral method with a single layer potential representation of eigenfunction. Both methods can possibly achieve spectral convergence. Furthermore, they both studied maximization of λ_k among star-shaped domains with a fixed area [1,7].

Mixed boundary problems were solved in [2,26] via isoparametric finite element method and the virtual element method, respectively. The error estimates for eigenvalues and eigenfunctions were derived. Another type of Steklov problem which is formulated as

$$\begin{cases} -\triangle u(\mathbf{x}) + u(\mathbf{x}) = 0 & \text{in} \quad \Omega, \\ \frac{\partial u}{\partial n} = \lambda u & \text{on} \quad \partial \Omega \end{cases}$$

was studied numerically in [5,6,23,30]. In [9], the authors look for a smooth open subset $A \subset \Omega$ that minimizes the first Steklov-like problem

$$\begin{cases} -\triangle u(\mathbf{x}) + u(\mathbf{x}) = 0 & \text{in} \quad \Omega \backslash \bar{A}, \\ \frac{\partial u}{\partial n} = \lambda u & \text{on} \quad \partial \Omega, \\ u = 0 & \text{on} \quad \partial A, \end{cases}$$

by using an algorithm based on finite element methods and shape derivatives. Furthermore, finite element methods have been also applied to the nonlinear Steklov eigenvalue problems [21] and methods of fundamental solutions were proposed lately to find a convex shape that has the least biharmonic Steklov eigenvalue [3].

The aim of this paper is two-fold. First, we develop numerical approaches to solve the forward problem of the Steklov eigenvalue problem by using spectral methods for complex formulations via conformal mapping approaches [10,20] for any given simply-connected planar domain. Second, we aim to find the maximum value of λ_k with a fixed area among simply-connected domains in two dimensions via a gradient ascent approach. To find optimal domains, we start with a chosen initial domain of any shape and deform the domain with the velocity which is obtained by calculating the shape derivative and choosing the ascent direction. In the complex formulation, the deforming domain is mapped to a fixed unit circle which allows spectral methods to solve the problem efficiently.

In Sections 2 and the formulations of the Steklov eigenvalue problem in the real plane \mathbb{R}^2 and the complex plane \mathbb{C} are described, respectively. Some known analytical solutions are provided and optimization of $\lambda_k \sqrt{|\Omega|}$ is formulated. In Section 4, computational methods based on Fourier series expansion are described. In Section 5, numerical results are presented. The summary and discussion are given in Section 6.

2. The Steklov eigenvalue problem on $\Omega \subset \mathbb{R}^2$

In this section, we discuss some known analytical solutions of the Steklov eigenvalue problem on simple geometric shapes and formulate the maximization of the *k*th Steklov eigenvalue with a fixed area constraint.

2.1. Some known analytical solutions

2.1.1. On a circular domain

By using the method of separation of variables, it is well known that the Steklov eigenvalues of a unit circle Ω [18] are given by

$$0, 1, 1, 2, 2, \ldots, k, k, \ldots$$

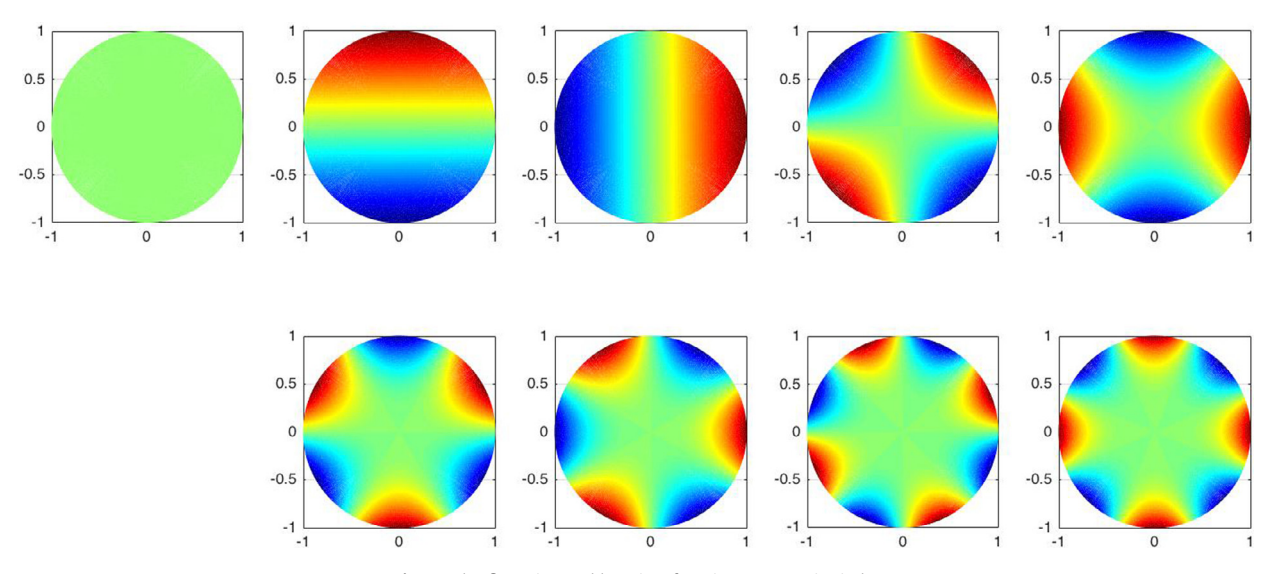


Fig. 1. The first nine Steklov eigenfunctions on a unit circle.

where $\lambda_0 = 0$ and its corresponding eigenfunction is a constant function and $\lambda_{2k} = \lambda_{2k-1} = k$ for $k \ge 1$ and their corresponding eigenfunctions are

$$u_{2k} = r^k \cos(k\theta), \ u_{2k-1} = r^k \sin(k\theta).$$

The first nine eigenfunctions are shown in Fig. 1.

2.2. On an annulus

When $\Omega = B(0,1) \setminus B(0,\epsilon)$, the Steklov eigenvalues can be found via the method of separation of variables [14]. The only eigenfunction which is radial independent satisfies

$$u(r) = \left(\frac{-(1+\epsilon)}{\epsilon \ln \epsilon}\right) \ln(r) + 1,$$

and the corresponding eigenvalue is

$$\lambda = \frac{1+\epsilon}{\epsilon} \ln(1/\epsilon).$$

The rest of the eigenfunctions are of the form

$$u_{\nu}(r,\theta) = (Ar^{k} + Br^{-k})H(k\theta), \quad k \in \mathbb{N}$$

$$\tag{4}$$

where A and B are constants and $H(k\theta) = \cos(k\theta)$ or $H(k\theta) = \sin(k\theta)$. The boundary conditions become

$$\frac{\partial}{\partial_r} u_k(1,\theta) = \lambda \, u_k(1,\theta),$$

$$\frac{\partial}{\partial_r} u_k(\epsilon,\theta) = -\lambda \, u_k(\epsilon,\theta),$$
(5)

which can be simplified to the following system

$$\begin{bmatrix} \lambda \epsilon^k + k \epsilon^{k-1} & \lambda \epsilon^{-k} - k \epsilon^{-k-1} \\ \lambda - k & \lambda + k \end{bmatrix} \begin{bmatrix} A \\ B \end{bmatrix} = \begin{bmatrix} 0 \\ 0 \end{bmatrix}.$$

To obtain nontrivial solutions, the determinant of the matrix needs to be zero. Thus Steklov eigenvalues are determined by the roots of the following polynomial

$$p_k(\lambda) = \lambda^2 - \lambda k \left(\frac{\epsilon + 1}{\epsilon}\right) \left(\frac{1 + \epsilon^{2k}}{1 - \epsilon^{2k}}\right) + \frac{1}{\epsilon} k^2, \quad k \in \mathbb{N}.$$
 (6)

Note that every root corresponds to a double eigenvalue. If $\epsilon > 0$ is smaller enough, for k = 1, we get the smallest eigenvalue

$$\lambda_1(\Omega) = \frac{1}{2\epsilon} \frac{1+\epsilon^2}{1-\epsilon} \left(1 - \sqrt{1 - 4\epsilon \left(\frac{1-\epsilon}{1+\epsilon^2}\right)^2} \right).$$

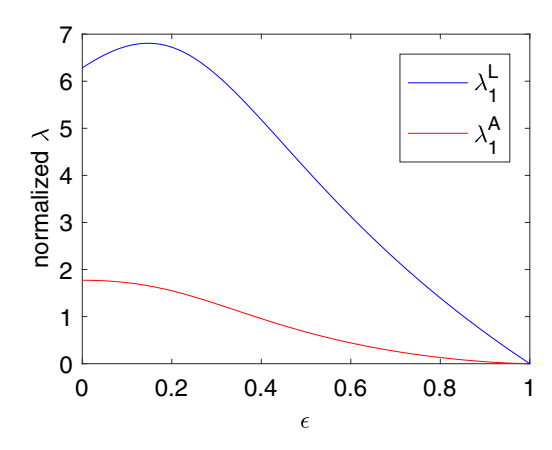


Fig. 2. The perimeter-scaled and area-scaled eigenvalues, λ_1^L and λ_1^A , on an annulus, respectively.

2.3. Shape optimization

It follows from (2) that the Steklov eigenvalues satisfy the homothety property $\lambda_k(t\Omega) = t^{-1}\lambda_k(\Omega)$. Instead of fixing the perimeter or the area, one can consider the following shape optimization problems

$$\lambda_k^{L\star} = \max_{\Omega \subset \mathbb{R}^2} \lambda_k^L(\Omega) \qquad \text{where } \lambda_k^L(\Omega) = \lambda_k(\Omega) |\partial \Omega| \tag{7}$$

and

$$\lambda_k^{A\star} = \max_{\Omega \subset \mathbb{R}^2} \lambda_k^A(\Omega) \qquad \text{where } \lambda_k^A(\Omega) = \lambda_k(\Omega) \sqrt{|\Omega|}. \tag{8}$$

As mentioned in the Introduction section, the solution of the perimeter-scaled eigenvalue problem (7) is known analytically for simply-connected domains. Thus, we focus only on the area-scaled eigenvalue problem as described in (8).

2.3.1. On an annulus

In Section 2.2 we get $\lambda_1(\Omega)$ on an annulus $\Omega = B(0,1) \setminus B(0,\epsilon)$. Thus, $\lambda_1^L = \lambda_1[2\pi(1+\epsilon)]$ is the first scaled eigenvalue with respect to the perimeter of the domain Ω . The perimeter scaled eigenvalue is not a monotone function in ϵ and it reaches the maximum value 6.8064 when $\epsilon = \epsilon^* \approx 0.1467$ [18] as shown in Fig. 2. On the other hand $\lambda_1^A = \lambda_1[\sqrt{\pi(1-\epsilon^2)}]$ is the first scaled eigenvalue with respect to the area of the domain Ω which turns out to be a monotone decreasing function in ϵ and it reaches the maximum value $\sqrt{\pi}$ when $\epsilon = 0$ as shown in Fig. 2.

2.3.2. Shape derivative

Here we review the concept of the shape derivative and assume regularity of the domain Ω . For more details, we refer the readers to [28]. The shape derivative of Steklov eigenvalue has been studied in [1,12]. Here we give the explicit formula of shape derivative of the area-scaled Steklov eigenvalue λ_k^{λ} .

Definition: Let $\Omega \subset \mathbb{R}^2$ be a bounded smooth open set and J be a functional on $\Omega \mapsto J(\Omega)$. Consider the perturbation $x \in \Omega \to x + tV \in \Omega_t$ where V is a vector field. Then the shape derivative of the functional J at Ω in the direction of a vector field V is given by

$$(J(\Omega))' = dJ(\Omega; V) = \lim_{t \downarrow 0} \frac{J(\Omega_t) - J(\Omega)}{t}$$
(9)

if the limit existed.

The shape derivative of area-scaled Steklov eigenvalue is given by the following proposition.

Proposition 1. Consider the perturbation $x \mapsto x + tV$ where V is a vector field in the Sobolev space $W^{3,\infty}(\Omega,\mathbb{R}^2)$ and denote $V_n = V \cdot \hat{n}$ where \hat{n} is the outward unit normal vector. Then a simple area-scaled Steklov eigenvalue λ_k^A satisfies the following formula

$$\left(\lambda_k^A(\Omega)\right)' = \sqrt{|\Omega|} \int_{\partial\Omega} \left(\left(|\nabla u|^2 - 2\lambda^2 u^2 - \lambda \kappa u^2 \right) + \lambda_k(\Omega) \frac{1}{2|\Omega|} \right) V_n \, ds. \tag{10}$$

where κ is the curvature of $\partial\Omega$ and u is the corresponding normalized eigenfunction satisfying (3).

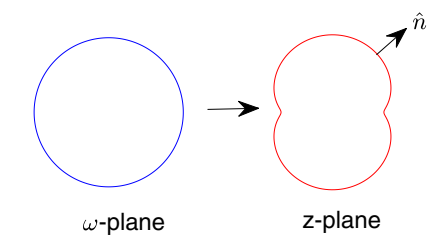


Fig. 3. The mapping from a unit circle on ω -plane to a simply-connected domain on z-plane.

Proof. By using the product rule, we have

$$(\lambda_k^A(\Omega))' = (\lambda_k(\Omega) \cdot \sqrt{|\Omega|})'$$

$$= (\lambda_k(\Omega))' \sqrt{|\Omega|} + \lambda_k(\Omega) \frac{1}{2\sqrt{|\Omega|}} |\Omega|'.$$
(11)

The shape derivative of Steklov eigenvalue [1,12] is found to be

$$(\lambda_k(\Omega))' = \int_{\partial\Omega} (|\nabla u|^2 - 2\lambda^2 u^2 - \lambda \kappa u^2) V_n \, ds \tag{12}$$

where κ is the curvature of $\partial\Omega$ and the shape derivative of the volume of Ω [28] is

$$|\Omega|' = \int_{\partial\Omega} V_n \, ds. \tag{13}$$

Plugging (12) and (13) into (11) concludes the proof. \Box

Thus the normalized velocity for the ascent direction can be chosen as

$$V_n = \left(|\nabla u|^2 - 2\lambda^2 u^2 - \lambda \kappa u^2 \right) + \lambda_k(\Omega) \frac{1}{2|\Omega|}. \tag{14}$$

Later we will show how to use this velocity V_n to find the optimal domain which maximizes the scaled kth Steklov eigenvalue with respect to the area for a given k.

3. The Steklov eigenvalue problem on the complex plane

3.1. On a simply-connected domain

In this section, we reformulate the Steklov eigenvalue problem on the unit circle on the complex plane $\mathbb C$ instead of on a simply-connected domain $\Omega \subset \mathbb R^2$. The following proposition provides the formulation.

Proposition 2. The Steklov eigenvalue problem (1) on a simply-connected domain $\Omega \subset \mathbb{R}^2$ with u which is twice continuously differentiable is equivalent to the complex formulation

$$\Re\{\omega\Psi_{\omega}\} = \lambda |f_{\omega}|\Re\{\Psi\} \qquad \text{on}|\omega| = 1,\tag{15}$$

where f is the mapping function from the interior of a unit circle on the complex plane $\mathbb C$ to the interior of Ω on $\mathbb R^2$ and Ψ is an analytic function with the real part u.

Proof. Due to the Riemann Mapping Theorem [4] that guarantees the existence of a conformal mapping between any two simply-connected domains, we denote $f = f(\omega)$ as the mapping function that maps the interior of a unit circle $|\omega| = 1$, where $w = re^{i\theta} = \xi + i\eta$ to the interior of Ω . Furthermore, on a simply-connected domain, every harmonic function u which is twice continuously differentiable and satisfies Laplace's equation is the real part of an analytic function, i.e., $u = \Re\{\Psi\}$ where Ψ is the complex potential and $\Re\{\Psi\}$ denotes the real part of the argument Ψ .

Parametrizing the boundary of the original domain Ω with $z(\theta) = x(\theta) + iy(\theta) = f(\omega)$, $|\omega| = 1$ as shown in Fig. 3. The outward unit normal is

$$\hat{n} = \left(\frac{\dot{y}}{\sqrt{\dot{y}^2 + \dot{x}^2}}, \frac{-\dot{x}}{\sqrt{\dot{y}^2 + \dot{x}^2}}\right),$$

where $\dot{x} = \frac{dx}{d\theta}$, $\dot{y} = \frac{dy}{d\theta}$ and the gradient of u is

$$\nabla_z u = u_x + i u_y$$
.

Thus the derivative in the normal direction is given by

$$\hat{n} \cdot \nabla_z u = \Im \left\{ \left(\frac{\dot{x} + i\dot{y}}{\sqrt{\dot{x}^2 + \dot{y}^2}} \right) (u_x - iu_y) \right\} = \Im \left\{ \frac{\dot{z}}{|f_\omega|} \overline{\nabla_z u} \right\}$$
(16)

where $\Im(\cdot)$ denotes the imaginary part of the argument. Since z = f(w), we have $\dot{z} = f_{\omega}\dot{\omega} = if_{\omega}\omega$ and $\overline{\nabla}_z u = \Psi_z = \Psi_{\omega}/f_{\omega}$. Thus, (16) becomes

$$\hat{\mathbf{n}} \cdot \nabla_{\mathbf{z}} u = \Im \left\{ \frac{i f_{\omega} \omega}{|f_{\omega}|} \frac{\Psi_{\omega}}{f_{\omega}} \right\} = \Re \left\{ \frac{\omega}{|f_{\omega}|} \Psi_{\omega} \right\} \quad \text{on } |\omega| = 1.$$

The boundary condition $\frac{\partial u}{\partial n} = \lambda u$ in (1) thus becomes

$$\Re\{\omega\Psi_{\omega}\} = \lambda |f_{\omega}|\Re\{\Psi\} \qquad \text{on}|\omega| = 1. \tag{17}$$

Note that $\lambda=0$ is an eigenvalue and its corresponding eigenfunction $u=\Re\{\Psi\}$ is a constant function. In this formulation, it is not necessary to solve the harmonic equation as the real part of an analytic function is always harmonic. However, it is required to know the mapping function $f(\omega)$ and solve the Eq. (17) on the unit circle. Sometimes it is not easy to find a conformal mapping that maps an unit circle to an arbitrary simply-connected domain analytically. When this happens, the Schwarz-Christoffel transformation [15] can be used to estimate the mapping.

3.2. Shape optimization problem

Here we first formulate the velocity in the complex plane \mathbb{C} and then derive the equation for the flow in the ascent direction (14).

Proposition 3. Denote $f(\omega, t)$ as the mapping function from the interior of a unit circle on the complex plane \mathbb{C} to the interior of a simply-connected domain Ω on \mathbb{R}^2 which is deformed by the normal velocity V_n . Then

$$V_n = \Re\left\{\frac{f_t|f_w|}{wf_w}\right\}.$$

Proof. By using the fact that $|\omega|^2 = \bar{\omega}\omega = 1$, we obtain

$$\frac{d}{dt}(\bar{\omega}\omega) = \bar{\omega}_t\omega + \bar{\omega}\omega_t = 2\Re\{\bar{\omega}_t\omega\} = 0.$$

Since the mapping function is $z = f(\omega, t)$, we have $\frac{dz}{dt} = f_t + f_\omega \omega_t$. The normal component of the velocity is given by

$$\begin{split} V_n &= \hat{n} \cdot V = \Im \left\{ \frac{i f_\omega \omega}{|f_\omega|} \overline{(f_\omega \omega_t + f_t)} \right\} = \Re \left\{ \frac{f_\omega \omega}{|f_\omega|} \overline{(f_\omega \omega_t + f_t)} \right\} \\ &= \Re \left\{ \frac{\overline{f_\omega \omega}}{|f_\omega|} (f_\omega \omega_t + f_t) \right\} = \Re \left\{ |f_\omega| \overline{\omega} \omega_t + \frac{f_t |f_\omega|}{\omega f_\omega} \right\} \\ &= \Re \left\{ \frac{f_t |f_\omega|}{\omega f_\omega} \right\}. \end{split}$$

Therefore, the flow in the ascent direction (14) becomes

$$\Re\left\{\frac{f_t|f_w|}{wf_w}\right\} = |\nabla u|^2 - 2\lambda^2 u^2 - \lambda \kappa u^2 + \frac{\lambda}{2|\Omega|},$$

where u is the normalized eigenfunction satisfying

$$\int_{\partial\Omega} u^2 ds = \int_{|\omega|=1} (\Re\{\Psi\})^2 |f_{\omega}| d\omega = 1. \tag{18}$$

Thus

$$\Re\left\{\frac{f_t}{wf_w}\right\} = R(f, \Psi),\tag{19}$$

where the right hand side function $R(f, \Psi)$ is

$$R(f, \Psi) = \frac{1}{|f_{\omega}|} \left(|\Psi_{\omega}|^2 \frac{1}{|f_{\omega}|^2} - 2\lambda^2 \Re(\Psi)^2 - \lambda \kappa \Re(\Psi)^2 + \frac{\lambda}{2|\Omega|} \right),$$

 $|\Omega|$ is the area of the given domain and the curvature is

$$\kappa = \frac{\Re\left\{\overline{\omega f_{\omega}}(\omega(\omega f_{\omega})_{\omega})\right\}}{|\omega f_{\omega}|^{3}}.$$
(20)

Now, since f is analytic in $|\omega| < 1$,

$$\frac{f_t}{\omega f_{\omega}}$$
 is analytic in $|\omega| < 1$.

By using the Poisson integral formula [4], the value of an analytic function in the domain $|\omega| < 1$ can be obtained in term of its real part evaluated on the unit circle. The Eq. (19) implies that

$$\frac{f_t}{\omega f_{\omega}} = \frac{1}{2\pi i} \oint_{|\omega'|=1} \frac{1}{\omega'} \frac{\omega' + \omega}{\omega' - \omega} R(f(\omega'), \Psi(\omega')) d\omega'$$
$$= R(f(\omega), \Psi(\omega)) + i\mathcal{H}\{R(f(\omega), \Psi(\omega))\}$$

where

$$\mathcal{H}[R(f(e^{i\theta}), \Psi(e^{i\theta}))] = \frac{1}{2\pi} \text{ p.v. } \int_{-\pi}^{\pi} \cot\left(\frac{\theta' - \theta}{2}\right) R(f(e^{i\theta'}), \Psi(e^{i\theta'})) d\theta'$$

is the Hilbert transform. Thus we have

$$f_t = \omega f_\omega(\Re(R(f(\omega), \Psi(\omega))) + i\mathcal{H}[R(f(\omega), \Psi(\omega))]) \tag{21}$$

which provides the deformation of the domain via the changes of the conformal mapping.

4. Numerical approaches for solving the Steklov eigenvalue problem

In this section, we discuss the details of numerical discretization. Assume f and Ψ are represented as series expansions, i.e.

$$f(w) = \sum_{k=-\infty}^{\infty} a_k \omega^k$$
 and $\Psi = \sum_{k=-\infty}^{\infty} c_k \omega^k$,

respectively. In Section 4.1, we discuss how to find Steklov eigenvalues and eigenfunctions on a given domain which is represented by $z = f(\omega)$, $|\omega| \le 1$. This requires to find eigenvalues λ and analytic functions Ψ whose real part are eigenfunctions in Eq. (17) for a given f. In Section 4.2, we discuss how to discretize Eq. (21) on a unit circle to obtain a system of ordinary differential equations (ODEs) of the coefficients $a_k(t)$ of $f(\omega, t)$ with a given initial guess of $a_k(0)$ of $f(\omega, 0)$.

4.1. Forward solvers

Given $f(w) = \sum_{k=-\infty}^{\infty} a_k w^k$, we solve (17) numerically on $|\omega| = 1$ by parametrizing the unit circle by using the angle θ $\omega = e^{i\theta}$, $\theta = [0, 2\pi)$.

Note that $a_k = 0$ for k < 0 as the domain is mapping to the interior of the unit circle, i.e. $|\omega| \le 1$. The derivative of f can be obtained as

$$f_{\omega} = \sum_{k=-\infty}^{\infty} k a_k \omega^{k-1}$$

and the magnitude of $|f_{\omega}| = \left(f_{\omega}\overline{f_{\omega}}\right)^{\frac{1}{2}}$ can be obtained in a series expansion again. Assume that the series expansion of $|f_{\omega}|$ is

$$|f_{\omega}| = \sum_{l=-\infty}^{\infty} d_{l} \omega^{l}.$$

Since $|f_{\omega}|$ is real, we must have $d_{l} = \overline{d_{-l}}$. Denote the expansion of Ψ as

$$\Psi = \sum_{k=-\infty}^{\infty} c_k \omega^k,$$

where $c_k = 0$ for k < 0 too. Plugging these series expansions into (17), we have

$$\sum_{k=-\infty}^{\infty} k(c_k - \overline{c_{-k}})\omega^k = \lambda \sum_{m=-\infty}^{\infty} \sum_{l=-\infty}^{\infty} (c_m + \overline{c_{-m}})d_l\omega^{m+l}.$$

We can then use the identity

$$\sum_{m=-\infty}^{\infty}\sum_{l=-\infty}^{\infty}(c_m+\overline{c_{-m}})d_l\omega^{m+l}=\sum_{k=-\infty}^{\infty}\sum_{m=-\infty}^{\infty}(c_m+\overline{c_{-m}})d_{k-m}\omega^k.$$

By matching the coefficients of ω^k , we have

$$\lambda \sum_{m=-\infty}^{\infty} (c_m + \overline{c_{-m}}) d_{k-m} = k(c_k - \overline{c_{-k}})$$
(22)

for all integer k. Denote the real and complex part of c_n , d_n by c_n^r , d_n^r and c_n^i , d_n^i , respectively, we then have

$$\lambda \sum_{m=-\infty}^{\infty} (c_m^r + ic_m^i + c_{-m}^r - ic_{-m}^i)(d_{k-m}^r + id_{k-m}^i) = k(c_k^r + ic_k^i - c_{-k}^r + ic_{-k}^i).$$

By comparing real and imaginary parts, we have

$$\begin{cases} \lambda \sum_{m=-\infty}^{\infty} c_m^r (d_{k-m}^r + d_{k+m}^r) + c_m^i (d_{k+m}^i - d_{k-m}^i) = k c_k^r, \\ \lambda \sum_{m=-\infty}^{\infty} c_m^r (d_{k-m}^i + d_{k+m}^i) + c_m^i (d_{k-m}^r - d_{k+m}^r) = k c_k^i. \end{cases}$$
(23)

In numerical computation, the series expansion is carried out numerically by truncating the series expansion to finite terms, and Fast Fourier Transform (FFT) is used to efficiently compute quantities in ω -plane and z-plane. Denote N as the total positive and negative modes used. We have

$$f(\omega) \approx \sum_{k=-N_2}^{N_2} a_k \omega^k = \sum_{k=-N_2}^{N_2} a_k e^{ik\theta}$$

and

$$f_{\omega} = \sum_{k=-N_2}^{N_2} k a_k \omega^{k-1}.$$

where $N_2 = N/2$. Denote

$$|f_{\omega}| = \sum_{l=-N}^{N} d_{l} \omega^{l},$$

where d_l , $-N \le l \le N$, are obtained by using the pseudo-spectral method. We use inverse Fourier transform (IFFT) to obtain f_{ω} in physical space and compute $|f_{\omega}|$ in physical space, then use FFT to get d_l in Fourier space. The aliasing of a nonlinear product is avoided by adopting the zero-padding.

The system of infinite Eq. (23) is approximated by the system of finite equations for $0:N_2$ -modes which gives

$$\lambda AC = BC, \tag{24}$$

where

$$\begin{split} A_{k+1,m+1} &= d_{k-m}^r + d_{k+m}^r, & \text{for} \quad 0 \leq k \leq N_2, \, 0 \leq m \leq N_2, \\ A_{k+1,m+N_2+1} &= -d_{k-m}^i + d_{k+m}^i, & \text{for} \quad 0 \leq k \leq N_2, \, 1 \leq m \leq N_2, \\ A_{k+N_2+1,m+1} &= d_{k-m}^i + d_{k+m}^i, & \text{for} \quad 1 \leq k \leq N_2, \, 0 \leq m \leq N_2, \\ A_{k+N_2+1,m+N_2+1} &= d_{k-m}^r - d_{k+m}^r, & \text{for} \quad 1 \leq k \leq N_2, \, 1 \leq m \leq N_2, \end{split}$$

and

$$\begin{split} B_{k+1,m+1} &= k\delta_{k,m}, & \text{for} \quad 0 \leq k \leq N_2, \, 0 \leq m \leq N_2, \\ B_{k+1,m+N_2+1} &= 0, & \text{for} \quad 0 \leq k \leq N_2, \, 1 \leq m \leq N_2, \\ B_{k+N_2+1,m+1} &= 0, & \text{for} \quad 1 \leq k \leq N_2, \, 0 \leq m \leq N_2, \\ B_{k+N_2+1,m+N_2+1} &= k\delta_{k,m}, & \text{for} \quad 1 \leq k \leq N_2, \, 1 \leq m \leq N_2, \end{split}$$

and

$$C = \begin{bmatrix} C^r \\ C^i \end{bmatrix},$$

where

$$C^{r} = \begin{bmatrix} c_{0}^{r} \\ c_{1}^{r} \\ c_{2}^{r} \\ \vdots \\ c_{N_{2}}^{r} \end{bmatrix}, \quad C^{i} = \begin{bmatrix} c_{0}^{i} \\ c_{1}^{i} \\ c_{2}^{i} \\ \vdots \\ c_{N_{2}}^{i} \end{bmatrix}.$$

By solving the linear system (24) we could find the coefficient vector C and its corresponding eigenvalue λ . We assign zero values for c_k^r and c_k^i for $k > N_2$. Thus the corresponding eigenfunction will be given by $u = \Re\{\Psi\} = \Re\{\sum_{-N_2}^{N_2} c_k \omega^k\}$.

Now, if we assume that the coefficients d_n are real we will be able to reduce the matrix size and solve the problem even more efficiently. In this case, we have

$$\begin{cases} \lambda \sum_{m=0}^{N_2} c_m^r (d_{k-m} + d_{k+m}) &= k c_k^r, \\ \lambda \sum_{m=1}^{N_2} c_m^i (d_{k-m} - d_{k+m}) &= k c_k^i. \end{cases}$$
(25)

The $0:N_2$ -modes approximation gives

$$\lambda A^r C^r = B^r C^r$$
, $\lambda A^i C^i = B^i C^i$.

where

$$A_{k+1,m+1}^r = d_{k-m} + d_{k+m}, \quad B_{k+1,m+1}^r = k\delta_{k,m} \quad \text{for} \quad 0 \le k \le N_2, 0 \le m \le N_2,$$

$$A_{k,m}^{i} = d_{k-m} - d_{k+m}, \quad B_{k,m}^{i} = k\delta_{k,m}, \quad \text{for} \quad 0 \le k \le N_2, 0 \le m \le N_2,$$

and

$$C^{r} = \begin{bmatrix} c_{0}^{r} \\ c_{1}^{r} \\ c_{2}^{r} \\ \vdots \\ c_{N_{2}}^{r} \end{bmatrix}, \quad C^{i} = \begin{bmatrix} c_{0}^{i} \\ c_{1}^{i} \\ c_{2}^{i} \\ \vdots \\ c_{N_{2}}^{i} \end{bmatrix}.$$

4.2. Optimization solvers

In this section, we discuss how to solve the dynamic Eq. (21) by method of lines and spectral method in the variable ω . The Eq. (21) is derived by finding the ascent direction of a simple area-scaled kth Steklov eigenvalue. While Steklov eigenvalues are not differentiable when they have multiplicity greater than one, in practice, eigenvalues computed numerically that approximate the Steklov eigenvalues of a domain are generically simple. In [1], the problem is reformulated to a minimax problem. In our implementation, we just pick one of the corresponding eigenfunctions when multiplicity of eigenvalue is greater than one numerically.

Given a conformal mapping $f(\omega,t)=\sum_{-N_2}^{N_2}a_k(t)\omega^k$, we use the method discussed in Section 4.1 to obtain kth eigenvalue λ_k , its corresponding eigenfunction $u_k=\Re\{\Psi\}$ where $\Psi(w,t)=\sum_{-N_2}^{N_2}c_k(t)\omega^k$. Notice that this eigenfunction is not normalized. To find the normalization constant, we compute the Fourier coefficient representation of

$$(\Re{\{\Psi\}})^2 |f_{\omega}| = \sum_{-N_2}^{N_2} b_k(t) \omega^k$$

via a pseudo-spectral method and then the normalization condition (18) is approximated by

$$\int_{|\omega|-1} (\Re\{\Psi\})^2 |f_{\omega}| d\omega \approx 2\pi b_0(t).$$

The normalized eigenfunction $u = \Re\{\tilde{\Psi}\}$ where

$$\tilde{\Psi}(w,t) = \sum_{-N_2}^{N_2} \frac{1}{\sqrt{2\pi b_0}} c_k(t) \omega^k = \sum_{-N_2}^{N_2} \tilde{c}_k(t) \omega^k.$$

The curvature term can be computed via the formula (20) by using the following expansions

$$\omega f_{\omega} = \sum_{-N_2}^{N_2} k a_k(t) \omega^k$$

$$\omega(\omega f_{\omega})_{\omega} = \sum_{-N_2}^{N_2} k^2 a_k(t) \omega^k.$$

The area term is obtained by

$$|\Omega| = \sum_{-N_2}^{N_2} \pi k |a_k|^2.$$

Plugging

$$|f_{\omega}| = \sum_{-N}^{N} d_l \omega^l, \quad \tilde{\Psi}_{\omega} = \sum_{-N_2}^{N_2} k \tilde{c}_k(t) \omega^k,$$

the eigenvalue, the curvature, and the area into the right hand side of (21), we obtain $R(f, \tilde{\Psi})$ in terms of Fourier series. All the nonlinear term is obtained by using pseudo-spectral method. We then use discrete Hilbert transform to find the complex conjugate of $R(f, \tilde{\Psi})$ and then compute the right hand side of (21). Denote the series expansion of the right hand side as

$$wf_{w}\big(R\big(f(\omega),\tilde{\Psi}(\omega)\big)+i\mathcal{H}\big[R\big(f(\omega),\tilde{\Psi}(\omega)\big)\big]\big)=\sum_{-N_{2}}^{N_{2}}r_{k}(t)\omega^{k}.$$

Note that r_k depends on time and a_k , $-N_2 \le k \le N_2$. Since $f_t(\omega,t) = \sum_{-\infty}^{\infty} a_k'(t)\omega^k$, the dynamic Eq. (21) becomes a system of N+1 nonlinear ODEs in Fourier Coefficients

$$a'_k(t) = r_k(t), -N_2 \le k \le N_2.$$
 (26)

5. Numerical results

In this section, we report the numerical implementation of aforementioned algorithms based on conformal mappings. The calculations are done on a 6-core 2.66 GHz Intel Xeon computer with 16 GB of RAM. MATLAB built-in function "fft" ("ifft") is used for forward (inverse) Discrete Fourier transform and "eigs" is used with default convergence criteria. The forward solver takes about 0.01 s to find eigenvalues and eigenfunctions when N = 256 is used for the number of Fourier modes. It takes about 20 s per 1000 iterations in the optimization solvers which include the time to compute eigenpairs and solve the system of ODEs. Note that the computational time does not increase when the calculations are done for domains with really large diameters as mapping functions will scale correspondingly. This is one of the advantages compared to the approaches based on fundamental solutions, boundary integral methods, or finite element methods.

5.1. Forward solvers

Here we first test our forward solvers on various domains to demonstrate the spectral convergence of the numerical approaches described in Section 4.1. We verify the accuracy of the code by testing the first 12 eigenvalues on smooth shapes.

5.1.1. Steklov eigenvalues on a unit disk

When we consider the unit circle, the mapping function is $f(\omega) = \omega$ which gives $|f_{\omega}| = 1$. Thus $d_0 = 1$ and $d_l = 0$ for all $l \neq 0$. The system of Eq. (25) becomes

$$\begin{cases} \lambda c_k^r = k c_k^r, & k = 0, 1, 2, 3, \dots \\ \lambda c_k^i = k c_k^i, & k = 1, 2, 3, \dots \end{cases}$$
 (27)

If $\lambda = 0$, $c_k^r = c_k^i = 0$ for all positive integer and c_0^r is an arbitrary constant. If λ is a particular integer k_1 , i.e., $\lambda = k_1$, we must have

$$c_k^r = c_k^i = 0$$
 for $k \neq k_1$,

and $c_{k_1}^r$ and $c_{k_2}^i$ are arbitrary constants. Thus, Steklov eigenvalue for the unit circle are

$$0, 1, 1, 2, 2, 3, 3, \ldots, k_1, k_1, \ldots$$

The scaled eigenvalues $\lambda_k^A(\Omega) = \lambda \sqrt{|\Omega|}$ are listed in Table 1. It is clear that spectral accuracy is observed from the numerical results and the errors only contain round off errors $O(10^{-16})$ on double-precision arithmetic.

Table 1 The first 12 eigenvalues $\lambda_k, k=0,\ldots,11$ for different numbers of grid points $N=2^n, n=4,5,12$ on a unit circle.

N	24	2 ⁵	212	Exact
λ_0	0	0	0	0
λ_1	1.772453850905515	1.772453850905515	1.772453850905515	1.772453850905516
λ_2	1.772453850905515	1.772453850905515	1.772453850905515	1.772453850905516
λ_3	3.544907701811031	3.544907701811031	3.544907701811031	3.544907701811032
λ_4	3.544907701811031	3.544907701811031	3.544907701811031	3.544907701811032
λ_5	5.317361552716547	5.317361552716547	5.317361552716547	5.317361552716548
λ_6	5.317361552716547	5.317361552716547	5.317361552716547	5.317361552716548
λ_7	7.089815403622062	7.089815403622062	7.089815403622062	7.089815403622064
λ_8	7.089815403622062	7.089815403622062	7.089815403622062	7.089815403622064
λ_9	8.862269254527577	8.862269254527577	8.862269254527577	8.862269254527579
λ_{10}	8.862269254527577	8.862269254527577	8.862269254527577	8.862269254527579
λ_{11}	10.634723105433094	10.634723105433094	10.634723105433094	10.634723105433096

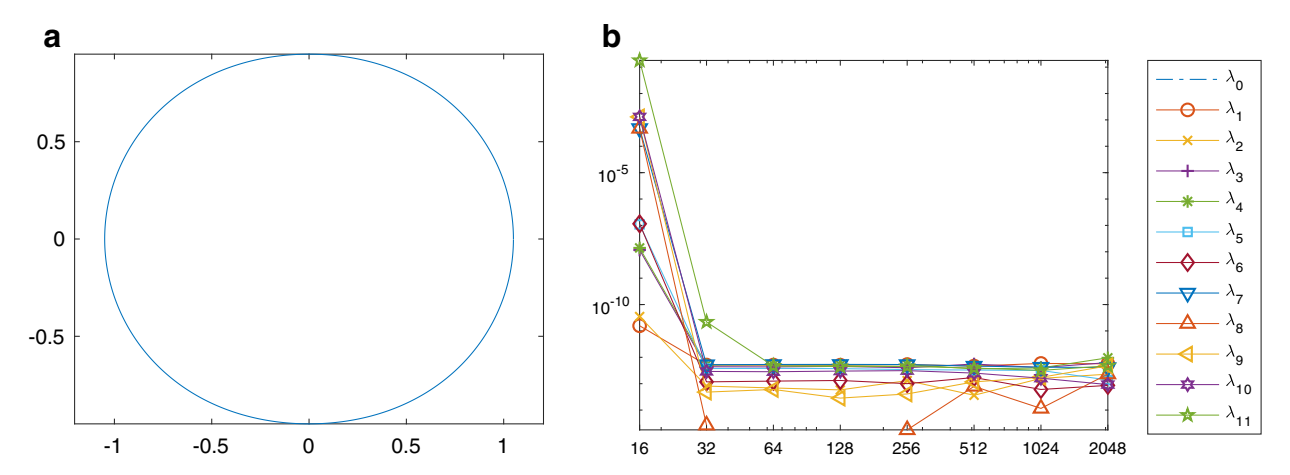


Fig. 4. (a) The 2-fold rotational symmetry shape with $f(w) = w + 0.05w^3$, $|\omega| \le 1$. (b) The log-log plot of errors for the first 11 non-zero eigenvalues versus number of grid points $N = 2^n$, $n = 4, \ldots, 11$.

Table 2 The first 12 eigenvalues $\lambda_k, k=0,\ldots,11$ for different numbers of grid points $N=2^n, n=4,\ldots,10,12$ on $f(w)=w+0.05w^3, |\omega|\leq 1$.

Ν	2^4	2^{5}	2^{6}	2 ⁷
λ_0	0	0	0	0
λ_1	1.643146123296456	1.643146123280263	1.643146123280263	1.643146123280268
λ_2	1.904409864808107	1.904409864772927	1.904409864772939	1.904409864772950
λ_3	3.509482564053473	3.509482552385534	3.509482552385528	3.509482552385548
λ_4	3.567218990382545	3.567218976359059	3.567218976359065	3.567218976359050
λ_5	5.298764914769874	5.298764805372437	5.298764805372433	5.298764805372439
λ_6	5.316931803045312	5.316931688027542	5.316931688027550	5.316931688027557
λ_7	7.074710761837761	7.074238491011210	7.074238491011200	7.074238491011197
λ_8	7.079268312074488	7.078792636301956	7.078792636301953	7.078792636301953
λ_9	8.846269410836159	8.844970458352126	8.844970458352138	8.844970458352106
λ_{10}	8.847598359495487	8.846297249970153	8.846297249970146	8.846297249970162
λ_{11}	10.793832137331764	10.614565359904542	10.614565359883139	10.614565359883118
Ν	28	2^{9}	2^{10}	2 ¹²
λ_0	0	0	0	0
λ_1	1.643146123296456	1.643146123280306	1.643146123280187	1.643146123280772
λ_2	1.904409864772878	1.904409864772972	1.904409864773167	1.904409864773008
λ_3	3.509482552385497	3.509482552385653	3.509482552385503	3.509482552385095
λ_4	3.567218976359074	3.567218976358907	3.567218976358941	3.567218976358544
λ_5	5.298764805372470	5.298764805372484	5.298764805372494	5.298764805372812
λ_6	5.316931688027525	5.316931688027596	5.316931688027485	5.316931688027425
λ_7	7.074238491011203	7.074238491011272	7.074238491011313	7.074238491011736
λ_8	7.078792636301955	7.078792636302032	7.078792636301965	7.078792636301953
λ_9	8.844970458352119	8.844970458352195	8.844970458352252	8.844970458352078
λ_{10}	8.846297249970174	8.846297249970114	8.846297249970023	8.846297249969862
λ_{11}	10.614565359883121	10.614565359883064	10.614565359882992	10.614565359882672

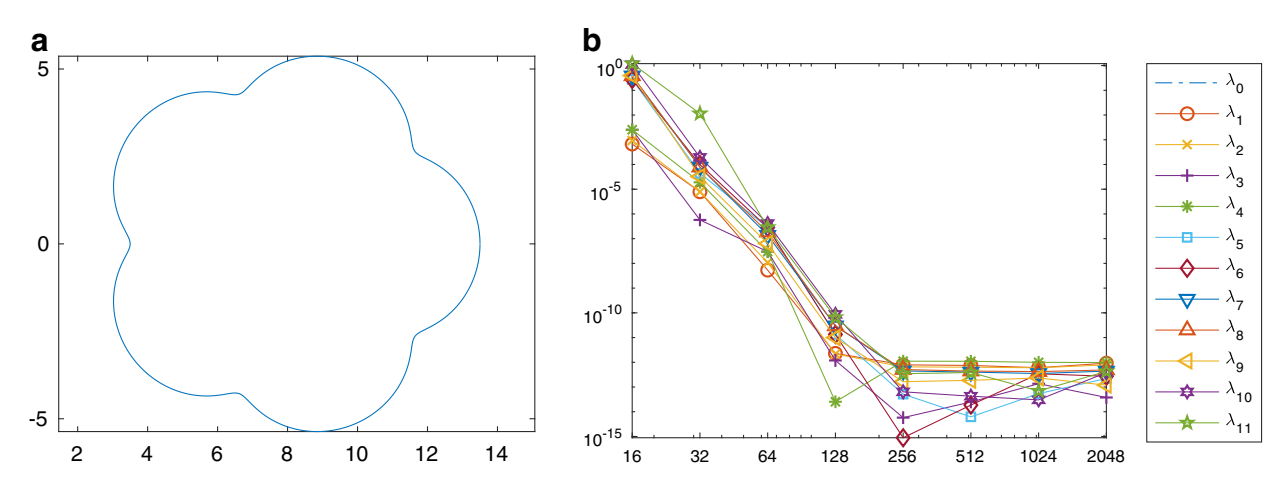


Fig. 5. (a) The 5-fold rotational symmetry shape with $f(w) = 8 + 5w + 0.5w^6$, $|\omega| \le 1$. (b) The log-log plot of errors for the first 11 non-zero eigenvalues versus number of grid points $N = 2^n$, $n = 4, \ldots, 11$.

Table 3 The first 12 eigenvalues λ_k , $k=0,\ldots,11$ for different numbers of grid points $N=2^n, n=4,\ldots,10,12$.

N	2^4	25	2^{6}	27
λ_0	0	0	0	0
λ_1	1.613981749710263	1.614659735134658	1.614651857980075	1.614651852652450
λ_2	1.615586942999712	1.614659740601958	1.614651863407194	1.614651852652469
l3	2.979901447266664	2.977376794062662	2.977377396867629	2.977377367030917
4	2.979920850098075	2.977396410343160	2.977377396867634	2.977377367030926
۱5	5.757902735512396	5.483423114699104	5.483379266795433	5.483378986137383
6	5.757963817902539	5.483478476088597	5.483379266795448	5.483378986137454
١7	7.091240897150815	6.707817046860952	6.707738934321966	6.707738797445765
18	7.092066936388594	6.707817092425547	6.707738981978962	6.707738797445767
وا	8.053537400023426	7.657772022224528	7.657739872866688	7.657739809188358
-10	10.114031561463605	9.019776832943990	9.019583333936978	9.019582922824695
11	11.339690354808871	10.150431507211664	10.138974110712084	10.13897382429239
V	28	2^{9}	2 ¹⁰	212
0	0	0	0	0
1	1.614651852650946	1.614651852650901	1.614651852650762	1.614651852650156
¹ 2	1.614651852650962	1.614651852650941	1.614651852650909	1.614651852650308
l3	2.977377367029736	2.977377367029755	2.977377367029867	2.977377367029730
4	2.977377367029792	2.977377367029804	2.977377367029905	2.977377367030901
15	5.483378986124044	5.483378986123986	5.483378986124047	5.483378986123992
6	5.483378986124095	5.483378986124115	5.483378986124439	5.483378986124096
١7	6.707738797416523	6.707738797416477	6.707738797416426	6.707738797416075
١8	6.707738797416656	6.707738797416588	6.707738797416567	6.707738797416147
وا	7.657739809178596	7.657739809178618	7.657739809178663	7.657739809178431
10	9.019582922738280	9.019582922738174	9.019582922738246	9.019582922738216
\ ₁₁	10.138973824227390	10.138973824227429	10.138973824227113	10.13897382422704

5.1.2. Steklov eigenvalues on a shape with 2-fold rotational symmetry

We use the mapping $f(w) = w + 0.05w^3$ to generate a shape with 2-fold rotational symmetry as shown in Fig. 4(a). In Table 2 we summarize the numerical results of Steklov eigenvalues. We use the eigenvalues computed by using 2^{12} grids as true eigenvalues and show the log-log plot of errors of the first 12 eigenvalues, i.e.

error=
$$|\lambda_k^N - \lambda_k^{2^{12}}|, k = 0, ..., 11,$$

versus number of grid points $N = 2^4, 2^5, \dots 2^{11}$ in Fig. 4(b). It is clear that the spectral accuracy is achieved.

5.1.3. Steklov eigenvalues on a shape with 5-fold rotational symmetry

We use the mapping $f(w) = 8 + 5w + 0.5w^6$ to generate a shape with 5-fold rotational symmetry as shown in Fig. 5(a). In Table 3, we use the eigenvalues computed by using 2^{12} grids as true eigenvalues and show the log-log plot of errors of the first 12 eigenvalues, i.e.

error=
$$|\lambda_k^N - \lambda_k^{2^{12}}|, k = 0, ..., 11,$$

versus number of grid points $N = 2^4, 2^5, \dots 2^{11}$ in Fig. 5(b). It is clear that the spectral accuracy is achieved.

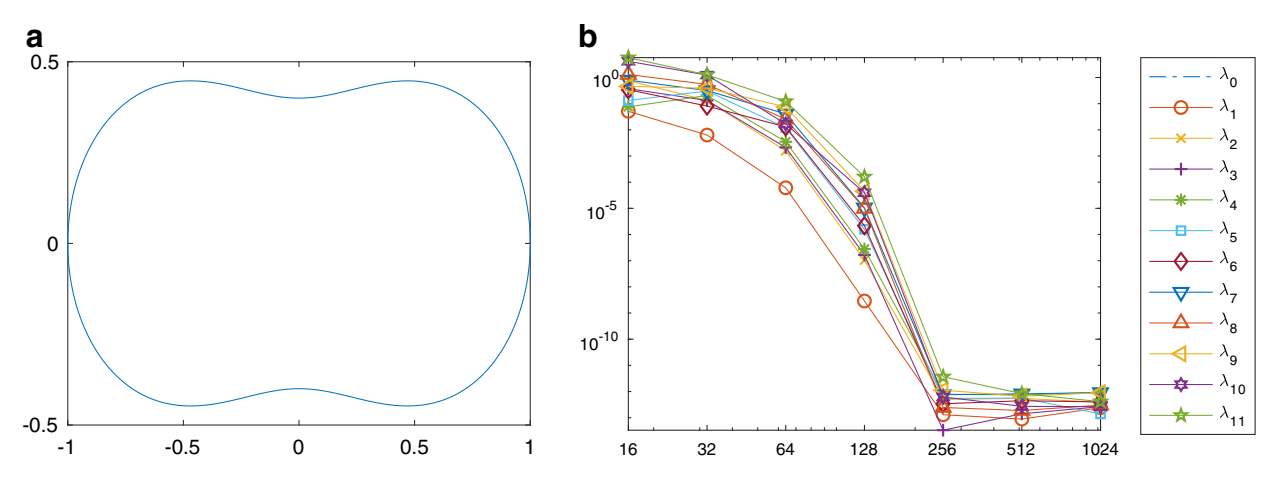


Fig. 6. (a) Cassini oval shape with $f(w) = \alpha w(\frac{1}{1+\alpha^2-(1-\alpha^2)w^2})^{\frac{1}{2}}$, $|\omega| \le 1$, and $\alpha = 0.4$. (b) The log-log plot of errors for the first 11 non-zero eigenvalues versus number of grid points $N = 2^n, n = 4, \ldots, 10$.

Table 4 The first 12 eigenvalues λ_k , $k=0,\ldots,11$ for different numbers of grid points $N=2^n, n=4,\ldots,10,12$.

N	2^4	2 ⁵	2^{6}	2^{7}
λ_0	0	0	0	0
λ_1	0.872759997500228	0.827902995301854	0.821644770560566	0.821583902061334
λ_2	2.124401456784662	2.756054635303737	2.886951802792420	2.888537681079042
λ_3	2.571449696110635	3.077030643209814	2.946970106404462	2.944846781799040
λ_4	3.265821414464841	3.136596486946471	3.338218243465505	3.341726009279193
λ_5	4.418763601488365	4.854880686612021	4.562691155962767	4.550749526079698
λ_6	5.378320687602239	4.955570564610835	5.023787664833372	5.036737477441735
λ_7	7.025574559110670	6.548839953593787	6.273463980936640	6.23306393320949
λ_8	7.626882523375537	6.870625350063478	6.299773422917886	6.325481073833819
λ_9	8.263730860061949	8.196071839036918	7.881197306312033	7.805852388999546
λ ₁₀	12.070450297339713	9.144520167848396	7.891680915128140	7.908376668589532
λ11	15.149068049247919	10.668830636509751	9.526157620343742	9.40438786949889
V	2^{8}	2^{9}	2 ¹⁰	2 ¹²
lο	0	0	0	0
λ1	0.821583899177118	0.821583899177077	0.821583899177230	0.821583899176988
λ_2	2.888537785769291	2.888537785769243	2.888537785769405	2.888537785769792
λ_3	2.944846615497959	2.944846615497851	2.944846615498256	2.977377367029730
λ4	3.341726289664183	3.341726289664230	3.341726289664046	3.341726289664970
λ_5	4.550747949109708	4.550747949109686	4.550747949110111	4.550747949110250
λ_6	5.036739639826136	5.036739639826031	5.036739639826076	5.036739639826476
λ7	6.233053526961343	6.233053526961285	6.233053526961188	6.23305352696210
λ8	6.325490988924451	6.325490988924394	6.325490988924508	6.32549098892420
λο	7.805807719443767	7.805807719443299	7.805807719443544	7.805807719442640
λ ₁₀	7.908416105951900	7.908416105952249	7.908416105952258	7.908416105952520
λ11	9,404227647278619	9.404227647275778	9.404227647275357	9,404227647274947

5.1.4. Steklov eigenvalues on a Cassini Oval.

All of aforementioned examples have finite terms expansion in ω . Here we show an example with infinite terms expansion in ω . The mapping $f(w) = \alpha w (\frac{2}{1+\alpha^2-(1-\alpha^2)w^2})^{\frac{1}{2}}$, where $\alpha=0.4$ is used to generate a Cassini Oval shape which is shown in Fig. 6(a). In Table 4 we use the eigenvalues computed by using 2^{12} grids as true eigenvalues and show the log-log plot of errors of the first 12 eigenvalues, i.e.

error=
$$|\lambda_k^N - \lambda_k^{2^{12}}|, k = 0, ..., 11,$$

versus number of grid points $N = 2^4, 2^5, \dots 2^{10}$ in Fig. 6(b). It is also clear that the spectral accuracy is achieved.

5.2. Optimization solvers

We solve the nonlinear system of ODEs (26) in Section 4.2 by using the forward Euler method with the time step h to obtain the solution at t + h. We can then repeat this procedure iteratively until it finds the optimal shape. The forward Euler method is chosen due to its simplicity. One can alternatively use adaptive time steps to integrate this system of ODEs. To

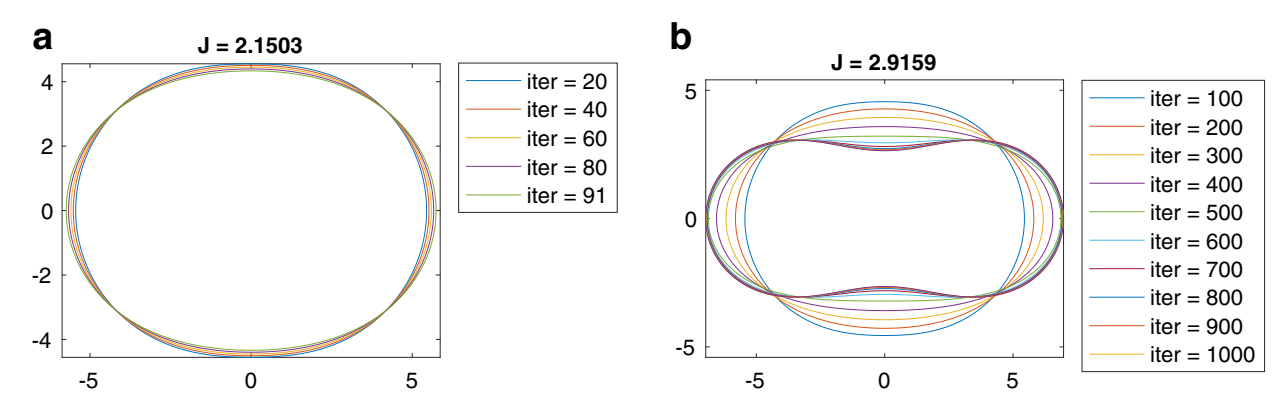


Fig. 7. Optimization of $\lambda_2^A(\Omega)$ without and with smoothing k are shown on (a) and (b), respectively.

Table 5 The optimization of λ_n^A , n = 2, ..., 7 for the first 12 eigenvalues.

λ_2^A	λ_3^A	λ_4^A
0	0	0
0.776986933500041	1.079861668314576	1.171320134341248
2.916071256633050	1.079861668314618	1.171320134341342
2.916071256753514	4.145300664720734	1.611279604736676
3.277492771330297	4.145300664720919	5.284432268416950
4.498623058633566	4.145300672478222	5.284433071016992
5.041166283776032	4.914601402877488	5.448244774262810
6.118061463397883	6.024394262148678	5.448244774262829
6.272697585592614	6.024394262148718	6.489865254319582
7.693637484890079	7.628170417847103	7.335382999100261
7.809873534891437	7.628170417847109	7.335382999100267
9.262237946100434	8.953916828143468	8.636733197287754
λ_5^A	λ_6^A	λ_7^A
0	0	0
1.239226322386241	1.265308570439713	1.291290525113730
1.239226322386290	1.265308570450229	1.291290525113829
1.945145428557867	2.117586845334797	2.250312782549877
1.945145428557917	2.117586845350534	2.250312782549968
6.496444238784153	2.427189796272854	2.777589136940805
6.496444238784278	7.644759577423688	2.777589137507856
6.496444784959914	7.644765127633966	8.846228548846659
6.732142619373287	7.771465908528654	8.846229141938371
6.732142619373318	7.771465908584982	8.846229145378315
8.128106267565293	7.979288943927369	9.050146643762274
8.803176067403113	7.979288943929372	9.050146643762337

prevent the spurious growth of the high-frequency modes generated by round-off error, we use 25th-order Fourier filtering and also filter out the coefficients which is below 10^{-14} as used in [27] after each iteration.

In Fig. 7(a), we show the evolution of optimization of λ_2^A with number of grid points N=256. We start with a shape with a two-fold symmetry $f(w)=w+0.5w^3$ whose $\lambda_2^A=1.7791$. The algorithm was able to deform the shape and increase the eigenvalue λ_2^A up to 2.1193. After that, the shape starts to generate kinks. Due to so-called crowding phenomenon [13], the accuracy of the conformal mapping will be effected and the shape will lose its smoothness. Thus, we avoid this problem by smoothing the curvature term κ in the z-plane based on the moving average method with span 5. Using this smoothing technique at each iteration helps us to achieve better results as shown in Fig. 7(b). In addition to smoothing, we also refine our time steps. We start with an initial time step h=0.1 and halve the time step for every time period T=100 and compute up to 5T. The optimal eigenvalues λ_k^A , $k=1,\ldots,7$ are summarized in Table 5 and the optimal shapes which have k-fold symmetry are shown in Fig. 8. These results match exactly to the ones reported in [8] which only showed two digits after the decimal point and are comparable to the ones reported in [1]. As observed in [1], the domain maximizing the kth Steklov eigenvalue has k-fold symmetry, and has at least one axis of symmetry. The k-th Steklov eigenvalue has multiplicity 2 if k is even and multiplicity 3 if $k \geq 3$ is odd. The first few nonzero coefficients of the mapping function f(w) of the optimal shapes are summarized in Table 6 for $\lambda_2^A - \lambda_7^A$. When optimizing λ_k^A , the optimal coefficients have nonzero values for a_{1+nk} where $n \in \mathbb{N}$.

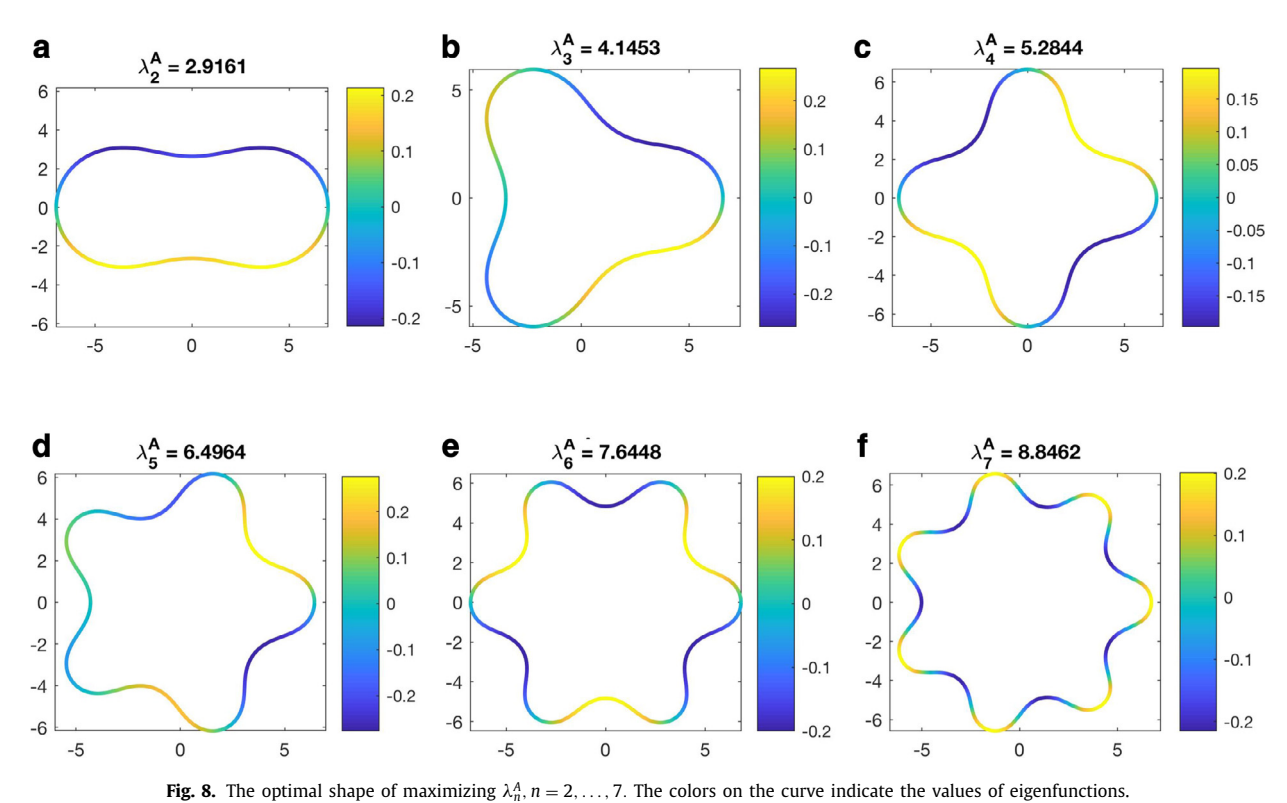


Table 6 The first few nonzero coefficients of the mapping function f(w) of the optimal shapes for

λ_2^A		λ_3^A		λ_4^A	
a_1	3.482625488377397	a_1	4.172312832330094	a_1	4.646184610628929
a_3	1.316760069380197	a_4	1.018987204748702	a_5	0.871201920168631
a_5	0.754288548863893	a_7	0.514733681728398	a_9	0.426363809028874
a_7	0.476336868618610	a_{12}	0.301544250312563	a_{13}	0.248913034789274
a_9	0.313178226238119	a_{15}	0.187629804532372	a_{17}	0.156013896896941
a_{11}	0.210225589908090	a_{18}	0.120456778256507	a_{21}	0.101460942653213
a_{13}	0.142829963279173	a_{21}	0.078773331531670	a_{25}	0.067443016703592
a_{15}	0.097776540001909	a_{24}	0.052126631797892	a_{29}	0.045465744838959
λ_5^A		λ_6^A		λ_7^A	
a_1	4.807404499929070	a_1	5.298095057399003	a_1	5.434176832482816
a_6	0.718033397997455	a_7	0.665755972200186	a_8	0.583992686042936
a_{11}	0.339254189743543	a_{13}	0.310395425069731	a_{15}	0.267954925737438
a_{16}	0.195019993266578	a_{19}	0.178491217642749	a_{22}	0.153351975823925
a_{21}	0.121279950688959	a_{25}	0.111622289351001	a_{29}	0.095872749417195
a_{26}	0.078576438618779	a_{31}	0.072927620185693	a_{36}	0.062767599076665
a_{31}	0.052167793728917	a_{37}	0.048905352581595	a_{43}	0.042229353541252
a ₃₆	0.035185234307276	a ₄₃	0.033346733965258	<i>a</i> ₅₀	0.028892884585296

6. Summary and discussion

We have developed a spectral method based on conformal mappings to a unit circle to solve Steklov eigenvalue problem on general simply-connected domains efficiently. Unlike techniques based on finite difference methods or finite elements methods which requires discretization on the general domains with boundary treatments, the method that we proposed only requires discretization of the boundary of a unit circle. We use a series expansion to represent eigenfunctions so that the discretization leads to an eigenvalue problem for Fourier coefficients. In addition, we study the maximization of areascaled Steklov eigenvalue λ_k^A based on shape derivatives and formulate this shape evolution in the complex plane via the gradient ascent approach. With smoothing technique and choices of time steps, we were able to find the optimal area-scaled eigenvalues λ_k^A for a given k.

As aforementioned, the optimization of Steklov eigenvalue problems on general non-simply-connected domains is a challenge open question. This will require robust and efficient forward solvers of Steklov eigenvalues and numerical techniques to perform shape optimizations which may involve topological changes. In the near future, we plan to explore the possibility in this direction with Level Set approaches.

Acknowledgments

We would like to thank the referees for their valuable comments.

Appendix A. The derivation of the mixed Steklov problem

Let us briefly review the derivation of the Steklov eigenvalue problem coming from the sloshing model which neglects the surface tension [19]. Consider the sloshing problem in a three-dimensional simply-connected container filled with inviscid, irrotational, and incompressible fluid. Choose Cartesian coordinates (x, y, z) so that the mean free surface lies in the (x, y)-plane and the z-axis is directed upwards. Denote \tilde{F} as the free fluid surface and B as the rigid bottom of the container. The governing equations in $\tilde{\Omega}$ of the sloshing model are

where V(x, y, z, t) is the fluid velocity, ρ is the density, p is the pressure, g is the gravity, and $\tilde{\Phi}(x, y, z, t)$ is the velocity potential. The last two equations lead to Laplace's equation

$$\triangle \tilde{\Phi} = 0 \quad \text{in} \quad \tilde{\Omega}.$$

The no penetration boundary condition at the rigid bottom of the container is

$$\nabla \tilde{\Phi} \cdot \hat{n}_B = 0 \quad \text{on} \quad B, \tag{28}$$

where \hat{n}_B is the outward unit normal to the boundary B and the dynamic boundary condition at the free surface $z = \tilde{\gamma}(x, y, t)$ is

$$\tilde{\gamma}_t + \nabla \tilde{\Phi} \cdot \nabla (\tilde{\gamma} - z) = 0.$$
 (29)

Rewriting the Navier–Stokes equation in terms of $ilde{\Phi}$ and using

$$(\mathbf{V} \cdot \nabla)\mathbf{V} = \frac{1}{2}\nabla |\mathbf{V}|^2 - \mathbf{V} \times (\nabla \times \mathbf{V}) = \frac{1}{2}\nabla |\mathbf{V}|^2,$$

we obtain the Bernoulli's equation

$$\nabla \left(\tilde{\Phi}_t + \frac{p}{o} + \frac{1}{2} \left| \nabla \tilde{\Phi} \right|^2 + gz \right) = 0. \tag{30}$$

Thus

$$\tilde{\Phi}_t + \frac{p}{\rho} + \frac{1}{2} \left| \nabla \tilde{\Phi} \right|^2 + gz = A(t) \tag{31}$$

where A(t) is an arbitrary function of t. By using the condition that the pressure p at the free surface equals to the ambient pressure p_{atm} and choosing $A(t) = \frac{p_{atm}}{o}$, we then have

$$\tilde{\Phi}_t + \frac{1}{2} \left| \nabla \tilde{\Phi} \right|^2 + gz = 0.$$

Therefore, we obtain the following partial differential equations

$$\Delta \tilde{\Phi} = 0 \qquad \text{in} \quad \tilde{\Omega},
\nabla \tilde{\Phi} \cdot \hat{n}_{B} = 0 \qquad \text{on} \quad B,
\tilde{\gamma}_{t} + \nabla \tilde{\Phi} \cdot \nabla (\tilde{\gamma} - z) = 0 \qquad \text{on} \quad \tilde{F},
\tilde{\Phi}_{t} + \frac{1}{2} |\nabla \tilde{\Phi}|^{2} + gz = 0 \qquad \text{on} \quad \tilde{F}.$$
(32)

Assuming the liquid motion is of small amplitude $z = \tilde{\gamma}(x, y, t)$ from the undisturbed free surface z = 0, we consider the following asymptotic expansion:

$$\tilde{\Phi}(x, y, z, t) = \Phi_0 + \epsilon \hat{\Phi}(x, y, z, t),
\tilde{\gamma}(x, y, t) = \gamma_0 + \epsilon \hat{\gamma}(x, y, t),$$

where Φ_0 is a constant velocity potential, $\gamma_0 = 0$, $\hat{\Phi}(x, y, z, t)$ and $\hat{\gamma}(x, y, t)$ represent perturbations, and $\epsilon > 0$ is a small parameter. Substituting these expansions in (32) gives

$$\Delta \hat{\Phi} = 0 \qquad \text{in} \qquad \tilde{\Omega},
\nabla \hat{\Phi} \cdot \hat{n}_{B} = 0 \qquad \text{on} \quad B,
\hat{\gamma}_{t} + \nabla \hat{\Phi} \cdot \nabla (\epsilon \hat{\gamma} - z) = 0 \qquad \text{on} \quad \tilde{F},
\hat{\Phi}_{t} + \epsilon \frac{1}{2} |\nabla \hat{\Phi}|^{2} + g \hat{\gamma} = 0 \qquad \text{on} \quad \tilde{F}.$$
(33)

It is well known that the time harmonic solutions of (33) with angular frequency α and phase shift σ are given by

$$\hat{\Phi}(x, y, z, t) = U(x, y, z)\cos(\alpha t + \sigma),$$

$$\hat{\gamma}(x, y, t) = \mu(x, y)\sin(\alpha t + \sigma),$$

where U(x, y, z) is the sloshing velocity potential and $\mu(x, y)$ is the sloshing height. Substitute these expansions into (33), transform the boundary conditions on \tilde{F} to F and the domain $\tilde{\Omega}$ to Ω by using Taylor expansion about z=0, and ignore high order terms. We then obtain

$$\begin{array}{cccc} \Delta U = 0 & & \text{in} & \Omega, \\ \nabla U \cdot \hat{n_B} = 0 & & \text{on} & B, \\ U_Z = \alpha \mu & & \text{on} & F, \\ \mu = \alpha \frac{U}{g} & & \text{on} & F. \end{array}$$

Thus, we obtain the mixed Steklov eigenvalue problem

$$\begin{array}{cccc} \Delta U = 0 & & \text{in} & \Omega, \\ \nabla U \cdot \hat{n_B} = 0 & & \text{on} & B, \\ U_Z = \lambda U & & \text{on} & F, \end{array}$$

where $\lambda = \alpha^2/g$.

When B is an empty set, the mixed Steklov eigenvalue problem is reduced to the classical Steklov eigenvalue problem (1). The Steklov spectrum satisfying (1) is also of fundamental interest as it coincides with the spectrum of the Dirichlet-to-Neumann operator. Consider a steady-state distribution of temperature u in a body Ω , which is a bounded open set with Lipschitz boundary $\partial \Omega$, for given temperature values on the boundary $\partial \Omega$. The resulting heat flux through the boundary which is linearly proportional to $\frac{\partial u}{\partial n}$ is uniquely determined. This can be described by the Dirichlet-to-Neumann operator Γ : $H^{\frac{1}{2}}(\partial \Omega) \to H^{-\frac{1}{2}}(\partial \Omega)$, given by the formula $\Gamma u = \partial_n(\mathbb{H}u)$, where $\mathbb{H}u$ denotes the unique harmonic extension of $u \in H^{\frac{1}{2}}(\partial \Omega)$ to Ω [11]. Here we use the standard notation that $H^m(\mathcal{M})$ is the Sobolev space of functions on \mathcal{M} with partial derivatives of order $\leq m$ in $L_2(\mathcal{M})$ for positive integer m. This space is defined also for negative m by duality and for fractional m by interpolation [24].

References

- [1] E. Akhmetgaliyev, C.-Y. Kao, B. Osting, Computational methods for extremal Steklov problems, SIAM J. Control Optim. 55 (2) (2017) 1226–1240.
- [2] A.B. Andreev, T.D. Todorov, Isoparametric finite-element approximation of a Steklov eigenvalue problem, IMA J. Numer. Anal. 24 (2) (2004) 309-322.
- [3] P.R.S. Antunes, F. Gazzola, Convex shape optimization for the least biharmonic Steklov eigenvalue, ESAIM Control Optim. Calc. Var. 19 (2) (2013) 385–403.
- [4] S.R. Bell, The Cauchy Transform, Potential Theory and Conformal Mapping, Chapman and Hall/CRC, 2015.
- [5] H. Bi, H. Li, Y. Yang, An adaptive algorithm based on the shifted inverse iteration for the Steklov eigenvalue problem, Appl. Numer. Math. 105 (2016)
- [6] H. Bi, Y. Yang, A two-grid method of the non-conforming Crouzeix–Raviart element for the Steklov eigenvalue problem, Appl. Math. Comput. 217 (23) (2011) 9669–9678.
- [7] B. Bogosel, The method of fundamental solutions applied to boundary eigenvalue problems, J. Comput. Appl. Math. 306 (2016) 265–285.
- [8] B. Bogosel, D. Bucur, A. Giacomini, Optimal shapes maximizing the Steklov eigenvalues, SIAM J. Math. Anal. 49 (2) (2017) 1645-1680.
- [9] J.F. Bonder, P. Groisman, J.D. Rossi, Optimization of the first Steklov eigenvalue in domains with holes: a shape derivative approach, Annali di Matematica Pura ed Applicata 186 (2) (2007) 341–358.
- [10] J.W. Brown, R.V. Churchill, M. Lapidus, Complex Variables and Applications, Vol. 7, McGraw-Hill New York, 1996
- [11] D. Colton, R. Kress, Inverse Acoustic and Electromagnetic Scattering Theory, 93, Springer Science & Business Media, 2012.
- [12] M. Dambrine, D. Kateb, J. Lamboley, An extremal eigenvalue problem for the Wentzell-Laplace operator, Annales de l'Institut Henri Poincaré (C) Non Linear Analysis 33 (2) (2016) 409-450.
- [13] T.K. Delillo, The accuracy of numerical conformal mapping methods: a survey of examples and results, SIAM J. Numer. Anal. 31 (3) (1994) 788-812.
- [14] B. Dittmar, Sums of reciprocal Stekloff eigenvalues, Math. Nachr. 268 (1) (2004) 44-49.
- [15] T.A. Driscoll, Schwarz-Christoffel Toolbox User's Guide, Technical Report, Cornell University, 1994.
- [16] A. Girouard, I. Polterovich, On the Hersch-Payne-Schiffer estimates for the eigenvalues of the Steklov problem, Funktsional. Anal. I Prilozhen 44 (2) (2010) 33-47.
- [17] A. Girouard, I. Polterovich, Shape optimization for low Neumann and Steklov eigenvalues, Math. Methods Appl. Sci. 33 (4) (2010) 501-516.
- [18] A. Girouard, I. Polterovich, Spectral geometry of the Steklov problem, J. Spectr. Theory 7 (2) (2017) 321–359.
- [19] R.A. Ibrahim, Liquid Sloshing Dynamics: Theory and Applications, Cambridge University Press, 2005.
- [20] C.-Y. Kao, F. Brau, U. Ebert, L. Schäfer, S. Tanveer, A moving boundary model motivated by electric breakdown: Ii. initial value problem, Phys. D Nonlinear Phenom. 239 (16) (2010) 1542–1559.

- [21] P. Kumar, M. Kumar, Simulation of a nonlinear Steklov eigenvalue problem using finite-element approximation, Comput. Math. Model. 21 (1) (2010)
- [22] N. Kuznetsov, T. Kulczycki, M. Kwaśnicki, A. Nazarov, S. Poborchi, I. Polterovich, B. Siudeja, The legacy of Vladimir Andreevich Steklov, Notices of the AMS 61 (1) (2014).
- [23] Q. Li, Y. Yang, A two-grid discretization scheme for the Steklov eigenvalue problem, J. Appl. Math. Comput. 36 (1) (2011) 129-139.

- [24] J.L. Lions, E. Magenes, Non-Homogeneous Boundary Value Problems and Applications, Vol. 1, Springer Science & Business Media, 2012.
 [25] H.C. Mayer, R. Krechetnikov, Walking with coffee: why does it spill? Phys. Rev. E 85 (4) (2012) 046117.
 [26] D. Mora, G. Rivera, R. Rodríguez, A virtual element method for the Steklov eigenvalue problem, Math. Models Methods Appl. Sci. 25 (08) (2015) 1421-1445.
- [27] Q. Nie, S. Tanveer, The stability of a two-dimensional rising bubble, Phys. Fluids 7 (6) (1995) 1292-1306.
- [28] J. Sokolowski, J.-P. Zolesio, Introduction to Shape Optimization, Springer, 1992.
- [29] R. Weinstock, Inequalities for a classical eigenvalue problem, J. Rat. Mech. Anal. 3 (6) (1954) 745–753.
- [30] H. Xie, A type of multilevel method for the Steklov eigenvalue problem, IMA J. Numer. Anal. 34 (2) (2013) 592-608.